



**AFRL-RX-WP-TP-2008-4338**

**A COUPLED EBSD/EDS METHOD TO DETERMINE THE  
PRIMARY-AND SECONDARY-ALPHA TEXTURES IN  
TITANIUM ALLOYS WITH DUPLEX  
MICROSTRUCTURES (PREPRINT)**

**A.A. Salem, M.G. Glavicic, and S.L. Semiatin**

**Metals Branch**

**Metals, Ceramics, and NDE Division**

**JULY 2007**

**Approved for public release; distribution unlimited.**

*See additional restrictions described on inside pages*

**STINFO COPY**

**AIR FORCE RESEARCH LABORATORY  
MATERIALS AND MANUFACTURING DIRECTORATE  
WRIGHT-PATTERSON AIR FORCE BASE, OH 45433-7750  
AIR FORCE MATERIEL COMMAND  
UNITED STATES AIR FORCE**

REPORT DOCUMENTATION PAGE				Form Approved OMB No. 0704-0188	
The public reporting burden for this collection of information is estimated to average 1 hour per response, including the time for reviewing instructions, searching existing data sources, gathering and maintaining the data needed, and completing and reviewing the collection of information. Send comments regarding this burden estimate or any other aspect of this collection of information, including suggestions for reducing this burden, to Department of Defense, Washington Headquarters Services, Directorate for Information Operations and Reports (0704-0188), 1215 Jefferson Davis Highway, Suite 1204, Arlington, VA 22202-4302. Respondents should be aware that notwithstanding any other provision of law, no person shall be subject to any penalty for failing to comply with a collection of information if it does not display a currently valid OMB control number. PLEASE DO NOT RETURN YOUR FORM TO THE ABOVE ADDRESS.					
1. REPORT DATE (DD-MM-YY) July 2007		2. REPORT TYPE Journal Article Preprint		3. DATES COVERED (From - To)	
4. TITLE AND SUBTITLE A COUPLED EBSD/EDS METHOD TO DETERMINE THE PRIMARY-AND SECONDARY-ALPHA TEXTURES IN TITANIUM ALLOYS WITH DUPLEX MICROSTRUCTURES (PREPRINT)				5a. CONTRACT NUMBER In-house	
				5b. GRANT NUMBER	
				5c. PROGRAM ELEMENT NUMBER 62102F	
6. AUTHOR(S) A.A. Salem (Universal Technology Corp.) M.G. Glavicic (UES, Inc.) S.L. Semiatin (AFRL/RXLMP)				5d. PROJECT NUMBER 4347	
				5e. TASK NUMBER RG	
				5f. WORK UNIT NUMBER M02R2000	
7. PERFORMING ORGANIZATION NAME(S) AND ADDRESS(ES) Universal Technology Corp. Metals Branch (AFRL/RXLMP) UES, Inc. Metals, Ceramics, and NDE Division Materials and Manufacturing Directorate Wright-Patterson Air Force Base, OH 45433-7750 Air Force Materiel Command, United States Air Force				8. PERFORMING ORGANIZATION REPORT NUMBER AFRL-RX-WP-TP-2008-4338	
9. SPONSORING/MONITORING AGENCY NAME(S) AND ADDRESS(ES) Air Force Research Laboratory Materials and Manufacturing Directorate Wright-Patterson Air Force Base, OH 45433-7750 Air Force Materiel Command United States Air Force				10. SPONSORING/MONITORING AGENCY ACRONYM(S) AFRL/RXLMP	
				11. SPONSORING/MONITORING AGENCY REPORT NUMBER(S) AFRL-RX-WP-TP-2008-4338	
12. DISTRIBUTION/AVAILABILITY STATEMENT Approved for public release; distribution unlimited.					
13. SUPPLEMENTARY NOTES Journal article submitted to the <i>Materials Science and Engineering A</i> . PAO Case Number: AFRL/WS 07-1628; Clearance Date: 12 Jul 2007. The U.S. Government is joint author of this work and has the right to use, modify, reproduce, release, perform, display, or disclose the work.					
14. ABSTRACT A method for separating the textures of primary alpha and secondary alpha in alpha/beta titanium alloys with a duplex microstructure was developed. Utilizing electron backscatter diffraction (EBSD) and energy-dispersive spectroscopy (EDS), the approach relies on the non-uniform partitioning of alloying elements between primary alpha and regions containing secondary-alpha lamellae and residual beta matrix phase. The method was evaluated using samples of Ti-6Al-4V for which vanadium partitions strongly to secondary alpha + beta regions. The technique thus provides a useful tool for quantifying the evolution of deformation texture in the primary alpha and transformation texture in secondary alpha formed via decomposition of the beta matrix following hot working or final heat treatment.					
15. SUBJECT TERMS titanium, texture, EBSD, microstructure, EDS					
16. SECURITY CLASSIFICATION OF:			17. LIMITATION OF ABSTRACT: SAR	18. NUMBER OF PAGES 36	19a. NAME OF RESPONSIBLE PERSON (Monitor) Sheldon L. Semiatin 19b. TELEPHONE NUMBER (Include Area Code) N/A
a. REPORT Unclassified	b. ABSTRACT Unclassified	c. THIS PAGE Unclassified			

# A coupled EBSD/EDS method to determine the primary- and secondary-alpha textures in titanium alloys with duplex microstructures

A.A. Salem<sup>a\*</sup>, M.G. Glavicic<sup>b</sup>, and S.L. Semiatin  
Air Force Research Laboratory, Materials and Manufacturing Directorate,  
AFRL/MLLM, Wright-Patterson AFB, OH 45433

<sup>a</sup>Universal Technology Corp., 1270 N. Fairfield Road, Dayton, OH 45432

<sup>b</sup>UES Inc., 4401 Dayton-Xenia Road, Dayton, OH 45433

## Abstract

A method for separating the textures of primary alpha ( $\alpha_p$ ) and secondary alpha ( $\alpha_s$ ) in alpha/beta titanium alloys with a duplex microstructure was developed. Utilizing electron backscatter diffraction (EBSD) and energy-dispersive spectroscopy (EDS), the approach relies on the non-uniform partitioning of alloying elements between primary alpha and regions containing secondary-alpha lamellae and residual beta matrix phase. The method was evaluated using samples of Ti-6Al-4V for which vanadium partitions strongly to secondary alpha + beta regions. The technique thus provides a useful tool for quantifying the evolution of *deformation* texture in the primary alpha and *transformation* texture in secondary alpha formed via decomposition of the beta matrix following hot working or final heat treatment.

*Keywords:* titanium, texture, EBSD, microstructure, EDS

## 1. Introduction

Titanium and its alloys are used extensively in the aerospace industry due to their high strength-to-weight ratio, excellent fracture toughness, and good corrosion/oxidation resistance. The allotropic transformation of titanium provides the foundation for the control of microstructure and thus properties via a plethora of thermomechanical

---

\* Corresponding author (e-mail: [ayman.salem@wpafb.af.mil](mailto:ayman.salem@wpafb.af.mil))

processes. Irrespective of the process, however, the overall goal is to control the volume fraction and morphology of the low-temperature alpha (hcp) and high-temperature beta (bcc) phases.

For applications limited by strength, ductility, and/or high-cycle fatigue properties, a duplex structure of primary (globular) alpha ( $\alpha_p$ ) in a transformed-beta matrix (comprising secondary-alpha ( $\alpha_s$ ) lamellae in the continuous beta matrix) is desirable. Such a structure is usually obtained via an ingot-metallurgy approach comprising hot working in the high-temperature beta field followed by a small increment of alpha/beta hot work, recrystallization of the worked beta grains in the beta field, rapid cooling from the beta field to form a colony microstructure within the prior-beta grains, and, finally, a second alpha/beta hot-working step to convert the lamellar microstructure thus formed into an equiaxed-alpha morphology [1]. More specifically, the second alpha/beta hot working operation gives rise to a structure (at the hot-working temperature) of  $\alpha_p$  particles in a matrix of beta which contains residual dislocation substructure. At room temperature, the exact form of the matrix phase depends on the cooling rate following hot working (or subsequent alpha/beta heat treatment) and thus the nature of the decomposition of the metastable beta-matrix phase. If the material is slow cooled from hot working (or heat treatment),  $\alpha_s$  lamellae (with a colony morphology) are formed; rapid cooling gives rise to martensitic alpha laths.

Increasing attention is now being focused on the formulation of physics-based models of microstructure/texture evolution and the resulting first- and second-tier properties. For alpha/beta titanium alloys with a duplex microstructure, for example, methods to determine the individual textures of  $\alpha_p$  and  $\alpha_s$  are required for the validation

of deformation and transformation texture models, respectively. Because the crystal structure and lattice parameters of primary and secondary alpha are identical, conventional x-ray or electron backscatter diffraction (EBSD) techniques can not be applied directly for this purpose. The objective of the current work, therefore, was to formulate and validate an EBSD-based technique for separating the individual textures. This approach was based on concurrent measurement of the local texture and composition using electron backscatter diffraction (EBSD) and energy-dispersive spectroscopy (EDS), respectively. The local composition variation enabled the automated binning of texture readings from the two different micro-constituents.

## **2. Background**

To put the current work into proper context, previously-developed techniques to separate the textures of  $\alpha_p$  and  $\alpha_s$  in alpha/beta titanium alloys are summarized in this section. For the most part, these prior methods have typically been indirect and consisted of the following steps: (i) measurement of the overall (primary + secondary) alpha texture using x-ray diffraction, neutron diffraction, or EBSD [2], (ii) determination of microstructure by optical or scanning-electron microscopy and separating primary and secondary alpha in the micrographs, (iii) correlating the specific regions for which microstructure and texture have been measured, and (iv) partitioning the texture data based on the difference in morphology of the primary and secondary alpha. In the duplex microstructure, the  $\alpha_p$  phase usually comprises equiaxed/globular particles, and  $\alpha_s$  are thin lamellae. When using scanning-electron microscope (SEM), the phases are readily distinguished using secondary-electron (SE) or backscattered-electron (BSE) imaging (Figure 1a, b, c). When using BSE imaging on a polished section, the  $\alpha_p$  and  $\alpha_s$  both

appear dark (due to atomic-number, or Z, contrast). The individual alpha lamellae in the  $\alpha_s$  are surrounded by layers of beta (or very fine martensitic alpha) which appear white (or gray) due to enrichment by beta stabilizers (such as vanadium or molybdenum) typically leading to a higher overall Z. Such a contrast between  $\alpha_p$  and  $\alpha_s+\beta$  can be revealed only under low magnification conditions and/or when the  $\alpha_s$  lamella are thin (Figure 1b).

Several different methods have been proposed to distinguish between primary and secondary alpha in micrographs and thus to correlate microstructural features and texture data [3-6]. For instance, Germain, *et al.* [3, 4] linked local orientations determined by the EBSD technique to corresponding positions in BSE images for Ti-6Al-4V. At *low* magnifications (at which the  $\alpha_s$  lamellae and the beta matrix are difficult to resolve),  $\alpha_p$  appears darker than  $\alpha_s$  (Figure 1c). The apparently lighter (gray) level of the  $\alpha_s$  results from the averaging effect at low magnification of low-Z secondary alpha and high-Z beta phase enriched in vanadium. The Germain, *et al.* technique is thus limited to low magnification BSE images in microstructures with very fine  $\alpha_s$  lamellae. Hence, this approach may be difficult to apply for duplex microstructures with thick  $\alpha_s$  lamellae or characterization using high magnification BSE images. Moreover, the technique also requires image rotation, resizing, translation, and shearing to match BSE images to EBSD inverse-pole-figure maps. Special software is required for the matching procedure due to differences in acquisition techniques.

Using a similar technique, Thomas, *et al.* [5] correlated EBSD texture information and microstructural information from *optical* images of the same area (e.g., Figure 1?). In this approach, the texture is measured first using EBSD. The sample is then etched to

locate and photograph the previously-scanned (“blank”) area. Because of the difference in acquisition techniques for texture and microstructure, special software was developed and applied to match EBSD maps and optical micrographs using rotation and resizing. Beside the time needed to etch samples and search for the scanned (blank) area, high resolution scans (step size  $< 0.5 \mu\text{m}$ , each with an acquisition time  $> 0.5 \text{ s}$ ) are required to produce enough carbon contamination to locate the blank after the etching. Therefore, characterization of a large area to obtain reasonable texture statistics may require long scans, fiducial marks for locating purposes, and extensive manual intervention,. In addition, the process is very sensitive to etching time; i.e., the marks left by the scanning process are lost if the etching time is too long.

To overcome some of shortcomings of other methods, Glavicic, *et al.* [6] suggested an indirect technique involving a heat treatment to eliminate the  $\alpha_s$  phase. In this approach, x-ray diffraction is used to measure the total ( $\alpha_p + \alpha_s$ ) texture. The separate  $\alpha_p$  texture is then determined on a portion of the sample which has been solution treated at a temperature high enough in the two-phase field to dissolve the  $\alpha_s$  and slow cooled to promote growth of the primary alpha without decomposition of the beta matrix (e.g., Figure 1e). The texture of the  $\alpha_p$  (weighted by its volume fraction in the initial duplex microstructure) is then subtracted from the  $\alpha_p + \alpha_s$  texture. The major shortcoming of this method concerns the implicit assumption that the heat treatment used to obtain the microstructure with only  $\alpha_p$  particles maintains the original texture of this phase; in other words, it is assumed that there is (a) no recrystallization or (b) preferential growth of particles with either different amounts of stored work from prior hot working operations or different texture components.

### 3. Material and experimental procedures

The present method to separate the textures of primary and secondary alpha was developed to overcome the shortcomings of earlier techniques. In brief, the approach is based on simultaneous, *in-situ* measurements of local orientation *and* composition within an SEM and eliminates the need for additional heat treatments or special post-processing software. Specifically, Kikuchi patterns and local composition data for the alpha phase are collected automatically inside an SEM using EBSD and energy-dispersive spectroscopy (EDS) detectors, respectively, for each point on the sample surface scanned by the electron beam. For this purpose, it is critical that both detectors be located on the same side of the microscope chamber (facing the surface of the sample), thus ensuring that both measurements are synchronized and come from the same material point during the scanning process. Texture is determined by off-line indexing of the Kikuchi patterns using OIM<sup>®</sup> data-analysis software [7].

#### 3.1. Material

Ti-6Al-4V was used to establish the usefulness of the new experimental technique for separating the textures of primary and secondary alpha. The starting material comprised a 32-mm-thick plate having a measured composition (in weight pct.) of 6.15 aluminum, 3.9 vanadium, 0.20 oxygen, 0.21 iron, 0.008 nitrogen, 0.01 carbon, 0.0031 hydrogen, and balance titanium.

#### 3.2. Experimental procedures

The Ti-6Al-4V program material was hot rolled at 955°C to a 3:1 reduction (effective strain of 1.15) followed by air cooling. The hot-rolled plate was then sectioned along the midplane, ground, and lightly electropolished at -20°C in a solution of 590 ml methanol and 60 ml perchloric acid. Following electropolishing, the sample was mounted

on the tilting stage inside an XL30 field-emission-gun scanning-electron-microscope (FEG-SEM). The microscope was operated at 20 kV and 7 nA with the stage tilted at an inclination of 70°. The EDS detector was fully retracted to avoid overexposure due to the large current used to collect the EBSD data.

Local Kikuchi patterns and chemical composition were collected using EBSD and EDS systems from EDAX [7]. A 0.3- $\mu\text{m}$  step size was used to cover an area measuring 80  $\mu\text{m}$  x 120  $\mu\text{m}$ . Different step sizes and larger areas (within the maximum of 25 mm x 50 mm associated with the microscope construction) were also utilized.

The texture results from the present technique were compared to those obtained using the x-ray diffraction (XRD) approach developed previously by Glavicic, *et al.* [6]. For this purpose, an additional sample was removed from the hot-rolled Ti-6Al-4V plate. The piece was cut into two equal sections. One half was analyzed in the as-hot-rolled condition (Figure 1b). The other was given a heat treatment to produce an alpha microstructure that was fully globular (Figure 1); i.e., it was annealed at 960°C (just above the rolling temperature) for one hour followed by furnace cooling. The volume fraction of primary alpha in the as-hot-rolled duplex microstructure was determined by analysis of BSE micrographs (Figure 1) taken in a Leica-Cambridge Stereoscan 360 FEG-SEM. Subsequently, both pieces were prepared for XRD on the RD-TD plane (at the midplane) of the rolled plate using standard metallographic techniques. XRD measurements were conducted using Cu K $\alpha$  radiation from an 18 kW rotating anode source, and textures were determined from measurements of partial (10 $\bar{1}$ 0), (0002), (10 $\bar{1}$ 1), (10 $\bar{2}$ 1), and (11 $\bar{2}$ 0) alpha-phase pole figures. In addition, partial (110) and (200) beta-phase pole figures were determined to enable a comparison of the  $\alpha_s$  texture

and the texture of the parent beta phase. The partial pole figures were completed using the orientation-distribution-function (ODF) analysis software in popLA (preferred orientation package from Los Alamos National Laboratory) [8].

To clarify the source of differences between the EBSD and XRD texture measurements, the former technique was also used to determine the texture of the starting (*unrolled*) Ti-6Al-4V program material after a 4-hour heat treatment at 955°C followed by furnace cooling or water quenching.

## **4. Results and discussion**

### *4.1. Microstructure observations*

Secondary-electron (SE) images revealed that the microstructure of the rolled Ti-6Al-4V sample consisted of 60 pct.  $\alpha_p$  particles within a matrix comprising colonies of  $\alpha_s$  lamellae separated by thin layers of the beta phase (Figure 2a). The shape of the  $\alpha_p$  particles was noticeably different from that of the  $\alpha_s$  lamella. On a lightly etched surface,  $\alpha_p$  appeared relatively equiaxed;  $\alpha_s$  comprised lamellae stacked in bundles (Figure 2a).

Observations based on the EBSD data shed additional insight into the nature of the microstructure. In particular, an inverse-pole-figure (IPF) map (Figure 2b) for the same area as the SE image revealed the orientations of the primary and secondary alpha phases. The misorientations across  $\alpha_s$  lamellae within a given colony were smaller than 3°. Hence, each  $\alpha_s$  bundle was recognized as a single grain by the OIM<sup>®</sup> software, and a single color was assigned to all lamella in the colony with no separating boundary. Based on the grain morphologies deduced from IPF maps alone, however, it was difficult to distinguish between  $\alpha_p$  particles and  $\alpha_s$  colonies. Furthermore, backscattered-electron (BSE) images (Figure 2g) as well as image-quality maps (Figure 2c) did not show clear

contrast between  $\alpha_p$  and  $\alpha_s$  as well, thus preventing the application of the technique of Germain, *et al.* [3, 4].

#### 4.2. Composition (EDS) results

The EDS results quantified the aluminum and vanadium concentration in different parts of the microstructure. In all cases, a high level of an alloying element was assigned a light color, and a lower level was represented with a darker color. The EDS map for aluminum (Figure 2e) showed a measurable variation in concentration. A comparison between aluminum EDS maps and SE images for the same areas confirmed that the lighter areas belonged to  $\alpha_p$  particles, and darker areas to  $\alpha_s$  lamellae. Specifically, higher aluminum concentrations (i.e., lighter colors) were found for  $\alpha_p$  particles, and lower concentration for  $\alpha_s$  lamellae (Figure 2e). The best contrast between  $\alpha_p$  and  $\alpha_s$  lamellae was revealed in EDS maps for vanadium (Figure 2f). The darker areas (lower vanadium) were associated with  $\alpha_p$  particles, and lighter areas with  $\alpha_s$  lamellae.

The qualitative EDS observations (Figures 2e, f) for the partitioning of alloying elements were as expected based on the phase equilibria determined by Semiatin, *et al.* [9] and Castro and Seraphin [10] for Ti-6Al-4V. In these previous efforts, it was shown that vanadium partitions preferentially to the beta phase between the alpha lamellae, and aluminum partitions preferentially to alpha. The partitioning is especially marked for vanadium; vanadium levels in the alpha and beta phases are of the order of 2 and 15 weight pct., respectively. The EDS measurements for  $\alpha_s$  regions are biased by the beta layers, which are enriched in vanadium and depleted in aluminum, thereby giving rise to the observed contrast.

Concentration histograms provided an automated means of separating regions of primary and secondary alpha. The aluminum concentration histogram revealed two overlapping Gaussian-like distributions, the lower one associated with  $\alpha_s$  lamellae and the higher one with  $\alpha_p$  particles (Figure 3b). The histogram for vanadium revealed two even more distinct Gaussian-like distributions with the lower one corresponding to  $\alpha_p$  particles and the higher one with  $\alpha_s$  lamellae (Figure 4a). For this reason, the local minimum at which the two Gaussian-like histograms for *vanadium* intersected was chosen as the point separating  $\alpha_p$  and  $\alpha_s$  for binning EDS, inverse-pole-figure, pole-figure, and image-quality data. In other words, any data point with a vanadium concentration lower or higher than that corresponding to point of intersection was considered to be  $\alpha_p$  or  $\alpha_s$ , respectively (Figure 4b). *Manual* separation of the EBSD data gave results similar to those obtained by partitioning the data automatically using the vanadium concentration (Figure 4a). Additional support for the technique was obtained from measurements of the volume fraction of  $\alpha_p$ . Values of ~57 and ~61 pct. were obtained using automated partitioning of IPF data (Figure 4b) and quantitative metallography on BSE images, respectively.

#### 4.3. Texture separation results for $\alpha_p$ and $\alpha_s$

Using the partitioning of vanadium to bin points corresponding to  $\alpha_p$  or  $\alpha_s$ , discrete (0001) pole figures for primary and secondary alpha were determined (Figure 5). The texture of the sample taken as a whole (i.e., the texture of  $\alpha_p + \alpha_s$ ) showed three major texture components (Figure 5a): a strong one along the rolling direction (RD) of the plate, a second weaker one along the transverse direction (TD) of the plate, and the weakest one consisting of four spots lying at approximately 45° to the RD and TD. The

separated texture showed that the (0001) pole figure of the  $\alpha_p$  phase had only one texture component in the RD direction (Figure 5b). A comparison of the separated (0001) pole figures (Figure 5b, c) revealed that the TD and the 45° texture components were associated with the  $\alpha_s$  phase (Figure 5c). In addition, both the  $\alpha_s$  and  $\alpha_p$  phases had a relatively strong texture component along the RD direction.

Insight into the nature of texture formation in the rolled plate was obtained from the microstructure of a specimen that was heat treated at the rolling temperature (955°C) and then water quenched. The BSE micrograph (Figure 6) indicated that only ~30 pct. of the microstructure was  $\alpha_p$  at the rolling temperature; the balance of the  $\alpha_p$  formed during cooling prior to the decomposition of the beta matrix to form alpha colonies ( $\alpha_s$ ). Due to the small amount of  $\alpha_p$  at 955°C, the majority of the strain imposed during the rolling process at 955°C was accommodated by the beta phase [11]. Hence, only small changes in the  $\alpha_p$  texture relative to that in the undeformed material would be expected due to deformation. On the other hand, the  $\alpha_s$  texture formed as a result of decomposition of heavily-worked beta. The interrelation of the  $\alpha_s$  and beta textures is discussed in the following section.

#### *4.4. Interpretation of beta-phase texture*

XRD measurements for the beta phase retained at room temperature (Figure 7) revealed a moderate texture. As mentioned in the previous section, a moderate-to-strong deformation texture may be expected in the beta phase because most of the strain is accommodated by it during rolling at 955°C. The decomposition of beta to form  $\alpha_s$  (plus a small amount of retained beta) typically follows the Burger relationship ((0001) $_{\alpha}$  parallel to (101) $_{\beta}$ ) [12]. As a result, the (0001)  $\alpha_s$  and (101) $_{\beta}$  pole figures would be

expected to be similar, as was observed (i.e., Figures 5c and 7). The similar locations of the different texture components in these pole figures provided support for the usefulness of the EBSD/EDS technique. However, there were some noticeable differences in the intensity of different components. The XRD  $(101)_\beta$  pole figure showed high intensities at the  $45^\circ$  location as well as at the RD and TD locations. By contrast, the  $\alpha_s$  (0001) pole figure showed the highest intensity at the TD direction and the lowest at  $45^\circ$ . Such differences are most likely related to preferential variant selection during the decomposition of the beta phase.

#### 4.5. Comparison of EBSD/EDS and XRD methods

Results from the EBSD/EDS method for separating the textures of primary and secondary alpha were compared with those obtained using the XRD method of Glavicic, *et al.* [6]. The overall texture of the  $\alpha$  phase ( $\alpha_p + \alpha_s$ ) was determined via XRD from the same sample used for the EBSD/EDS technique. The (0001) pole figure for this sample (Figure 8a) showed the same three components as in the EBSD/EDS measurement. However, the magnitude of the XRD TD component was greater than that of the RD component, in contrast to the findings from the EBSD/EDS measurement (Figure 5a). Similarly, the texture of the rolled sample heat treated at  $955^\circ\text{C}$  and furnace cooled to obtain a microstructure of equiaxed alpha (Figure 8b) exhibited a very strong RD component ( $\sim 2.5$  times as strong as the EBSD/EDS measurement) as well as very weak TD and  $45^\circ$  components which had been absent in the EBSD/EDS case. By subtracting the measured XRD  $\alpha_p$  texture (weighted by its volume fraction in the rolled sample) from the XRD  $\alpha_p + \alpha_s$  measurement, an estimate of the  $\alpha_s$  texture was obtained (Figure 8c). The

XRD (0001) pole figure so determined showed moderate TD and 45° components as did the EBSD/EDS sample, but lacked the RD component.

Several sources of the difference in the EBSD/EDS and XRD textures can be postulated. These factors include the overlap of the beta- and alpha-phase peaks in XRD data and the possible growth of different  $\alpha_p$  components during the heat treatment process used in the Glavicic, *et al.* method to obtain the  $\alpha_p$  texture. With regard to the first possibility, (110) pole figure of the beta phase may be expected to be superimposed on and thus “contaminate” (0001) pole-figure data of the alpha phase (for  $\alpha_p+\alpha_s$  as well as  $\alpha_p$ ) in Ti-6Al-4V due to the proximity of the  $(110)_\beta$  and  $(0001)_\alpha$  diffraction peaks. This contamination may be the source of the TD and 45° components in the XRD  $\alpha_p$  (0001) pole figure, which are not found in the EBSD/EDS measurement. From a quantitative standpoint, however, the degree of contamination depends on the volume fraction of beta retained in Ti-6Al-4V at room temperature (~6 pct.).

The higher intensity in the TD direction of the XRD  $\alpha_p$  pole figure compared to that for the EBSD/EDS pole figure may be due to the preferential growth of  $\alpha_p$  texture component along the TD direction during the heat treatment and furnace cooling. Evidence for such an effect is presented in the following section.

#### *4.6. Effect of slow cooling on preferential growth of primary alpha*

The major assumption of the XRD method to separate the  $\alpha_p$  and  $\alpha_s$  textures [5] is that the  $\alpha_p$  texture is preserved during high temperature solution treatment of the  $\alpha_s$  and slow cooling that gives rise to epitaxial growth of the  $\alpha_p$ . However, observed differences between the room-temperature texture of  $\alpha_p$  determined by EBSD (Figure 5b) and that

measured by XRD on a sample slow cooled following solution treatment (Figure 8b) cast doubt on this assumption.

The microstructure and texture of the starting (*unrolled*) Ti-6Al-4V program material after a 4-hour heat treatment 955°C followed by either water quenching or furnace cooling to room temperature provided further insight into this assumption and the possible growth of weak  $\alpha_p$  texture components during slow cooling from high-temperature solution treatment. The microstructure of the water quenched (WQ) sample revealed 30 pct.  $\alpha_p$  particles (dark) surrounded by martensite (Figure 9a). On the other hand, the furnace-cooled (FC) sample revealed 93 pct. of  $\alpha_p$  particles in a matrix of retained beta (Figure 9b).

The EBSD/EDS technique was used to determine the  $\alpha_p$  texture for the FC sample. However, an alternate EBSD binning technique using image-quality (IQ) maps was found to be necessary for the WQ sample which contained a large volume fraction (~70 pct.) of martensite. The high dislocation density in martensitic alpha results in a very low IQ during the indexing of EBSD Kikuchi patterns. For the WQ sample, an OIM<sup>®</sup> IQ threshold of 200 was found to provide an accurate separation of data for the primary and martensitic alpha. Such a threshold yielded volume fractions of the phases in excellent agreement with quantitative metallography (using SEM BSE images) and an  $\alpha_p$  texture identical to that derived by the tedious, manual-separation technique.

The  $\alpha_p$  textures of the WQ and FC samples measured by EBSD over areas as large as 5.6 mm x 1.2 mm and in 10 different randomly-chosen areas of the sample revealed distinctive differences (Figure 10). Based on a 1.2 mm x 1.2 mm scan, for example, the WQ sample (Figure 10a) had only one texture component comprising basal

poles along the RD. This  $\alpha_p$  texture is thus similar to that *after* rolling at 955°C (Figure 5b) and supports the hypothesis that the primary alpha underwent relatively little strain during hot rolling high in the alpha/beta phase field. By contrast, the unrolled FC sample (Figure 10b) had two *additional* texture components, one along the TD with intensity greater than  $\sim 9 \times$  random and components at 45° to the RD and TD with an intensity as high as  $4 \times$  random. These results thus strongly suggest that furnace cooling of the Ti-6Al-4V program material from a high solution temperature resulted in preferential growth of certain  $\alpha_p$  components which were initially very weak.

The effect of water quenching versus furnace cooling on the  $\alpha_p$  texture was further elucidated by measuring the texture over the *entire* sample surface by both EBSD and XRD. In particular, the  $\alpha_p$  texture measured by EBSD for an area measuring 20 mm x 4.8 mm revealed similar and distinctive differences between the WQ and the FC samples (Figure 11) as in the smaller-area scans. Specifically, the basal texture along the TD was very strong for the FC sample ( $\sim 14 \times$  random), but much weaker for the WQ sample ( $\sim 3$  times random). On the other hand, the FC sample had a lower-intensity basal texture along the RD ( $< 9 \times$  random) in comparison to that for the WQ sample ( $\sim 13$  times random).

Further examination of the EBSD results revealed that the texture component at 45° to the RD and TD was much weaker in large-area (20 mm x 4.8 mm) scans (Figure 11) compared to smaller-area (1.2 mm x 1.2 mm) scans (Figure 10). This difference can be explained by microtexture found in the unrolled WQ and FC samples, as illustrated by RD IPF maps (Figures 12 and 13). The microtexture was more pronounced in the FC

sample (Figure 12b and 13b), lending credence to the hypothesis that furnace cooling results in preferential growth of certain  $\alpha_p$  texture components.

XRD gave similar results for the  $\alpha_p$  texture of the FC sample. However, XRD determination of the  $\alpha_p$  texture for the WQ sample was not possible because of the presence of the large volume fraction (~ 70 pct.) of martensitic alpha whose diffraction peaks overlap those of the  $\alpha_p$  phase.

Several sources of preferential growth of the primary-alpha particles can be hypothesized. First, if the TD/45° textures are associated with globular particles which are *smaller* than those containing the RD texture, faster diffusional growth of the former during furnace cooling would be expected [9]. Second, a variation in morphology would affect the rates of growth of alpha particles during cooling. As discussed recently [13], the growth of remnant lamellar plates can be much slower than globular particles, the exact difference depending on the size of the particles and the thickness and the diameter-to-thickness ratio of the plates. Such differences in size or morphology of the primary alpha could easily be developed during breakdown rolling of a lamellar microstructure. Alpha plates whose c-axis is along the RD would be difficult to deform/spheroidize during deformation and thus tend to retain their morphology [14]. On the other hand, alpha plates whose c-axis is along the TD (or 45° to the RD and TD) would deform and spheroidize readily [14]. Such possibilities are now under investigation.

## **5. Summary and conclusions**

An EBSD/EDS method to separate the textures of primary alpha and secondary-alpha colonies in alpha-beta titanium alloys with a duplex microstructure was developed. This technique is based on binning each discrete EBSD measurement according to its

chemical composition as determined by simultaneous EDS. The approach was applied to hot-rolled Ti-6Al-4V in which the partitioning of vanadium provides the most noticeable signature for automated discrimination of primary-alpha particles ( $\alpha_p$ ) and the secondary-alpha colonies ( $\alpha_s$ ), the latter formed by decomposition of beta phase during cooling. The results for this material showed the following:

1. The primary-alpha (deformation) texture is aligned with the rolling direction.
2. The secondary-alpha (transformation) texture was correlated (through the Burgers relation between beta and alpha) to the deformation texture of the beta phase with principal components along the TD and at  $\sim 45^\circ$  to the RD and TD.
3. Quantitative differences in the intensity of specific components in the  $\alpha_s$  and parent beta textures suggested preferential variant selection during the transformation.
4. Furnace cooling from 955°C may cause preferential growth of weak primary-alpha texture components and lead to noticeable microtexture.
6. For water-quenched samples containing a large volume fraction of martensitic alpha, a binning technique similar to EBSD/EDS, but based on image quality, may be used for automated texture separation.

*Acknowledgements-* This work was conducted as part of the in-house research activities of the Metals Processing Group of the Air Force Research Laboratory's Materials and Manufacturing Directorate. The support and encouragement of the Laboratory management and the Air Force Office of Scientific Research (Dr. B.P. Conner, program manager) are gratefully acknowledged. The assistance of R. Wheeler in conducting the

experimental work is much appreciated. Two of the authors were supported through Air Force Contracts F33615-03-D-5801 (AAS) and FA8650-04-D-5235 (MGG).

## References

1. G. Lutjering, *Materials Science and Engineering A* A243 (1998) 32-45.
2. U. F. Kocks, C. N. Tome, H.-R. Wenk, *Texture and Anisotropy*, Cambridge University Press, Cambridge, United Kingdom, 1998, pp. 129-176.
3. L. Germain, N. Gey, M. Humbert, A. Hazotte, P. Bocher, M. Jahazi, *Materials Characterization* 54 (2005) 216-222.
4. L. Germain, N. Gey, P. Bocher, M. Jahazi, *Material Science Forum* 495-497 (2005) 663-668.
5. M. J. Thomas, B.P. Wynne, W. M. Rainforth, *Materials Characterization* 55 (2005) 388-394.
6. M. G. Glavacic, J. D. Miller, S. L. Semiatin, *Scripta Materialia* 54 (2006) 281-286.
7. EDAX, Inc., 392 East 12300 South, Suite H., Draper, UT 84020.
8. Los Alamos Polycrystal Plasticity Code, Los Alamos National Laboratory, Report LA-CC-88-6, 1988.
9. S.L. Semiatin, S.L. Knisley, P.N. Fagin, F. Zhang, D.R. Barker, *Metall. Mater. Trans. A* 34A (2003) 2377-2386.
10. R. Castro, L. Seraphin, *Mém. Sci. Rev. Metall.* 63 (1966) 1025-1058.
11. S.L. Semiatin, F. Montheillet, G. Shen, J.J. Jonas, *Metall. Mater. Trans. A* 33A (2002) 2719-2727.
12. W.G. Burgers, *Physica* 1 (1934) 561-586.

13. S.L. Semiatin, T.M. Lehner, J.D. Miller, R.D. Doherty, D.U. Furrer, *Metall. Mater. Trans. A*, 38A (2007) in press.
14. T.R. Bieler, S.L. Semiatin, *Inter. J. Plasticity*, 18 (2002) 1165-1189.

### Figure captions

Figure 1. Ti-6Al-4V microstructures: (a) SEM secondary-electron image for material with a duplex microstructure of globular  $\alpha_p$  and colonies of  $\alpha_s$ , (b) low magnification backscattered-electron (BSE) image revealing  $\alpha_p$  particles as dark areas and  $\alpha_s$  colonies as light gray areas, (c) high magnification BSE image revealing the similarity in darkness of both  $\alpha_p$  particles and the  $\alpha_s$  in the lamellar colonies, (d) optical micrograph of electropolished-and-etched surface revealing  $\alpha_p$  particles and  $\alpha_s$  colonies and (e) BSE image of the sample after epitaxial growth of the  $\alpha_p$  particles via furnace cooling from the solution temperature.

Figure 2. SEM results for an electropolished sample of hot-rolled Ti-6Al-4V: (a) secondary-electron image, (b) normal-direction inverse-pole-figure map showing indistinguishable  $\alpha_p$  and  $\alpha_s$  phases, (c) image-quality map of the same area with no clear difference between  $\alpha_s$  and  $\alpha_p$  phases, and EDS maps for (d) aluminum and (e) vanadium. In the EDS maps (d, e), dark or light shading is associated with lower or higher concentrations, respectively of the particular alloying elements.

Figure 3. Aluminum histogram determined by EDS.

Figure 4. Separation of  $\alpha_p$  and  $\alpha_s$  using vanadium partitioning: (a) EDS histogram (b) the corresponding microstructure partitioned based on vanadium content. In (b),  $\alpha_s$  colonies are painted blue.

Figure 5. Alpha-phase (0001) pole figures for hot-rolled Ti-6Al-4V determined by the EBSD/EDS technique and vanadium partitioning: (a)  $\alpha_p + \alpha_s$  texture, (b)  $\alpha_p$  particles, and (b)  $\alpha_s$  colonies.

Figure 6. Backscattered-electron image of the microstructure developed in undeformed Ti-6Al-4V during solution treatment at the rolling temperature (955°C) followed by water quenching.

Figure 7. Beta-phase (110) pole figure for hot-rolled Ti-6Al-4V determined by XRD.

Figure 8. Alpha-phase (0001) pole figures for hot-rolled Ti-6Al-4V determined using the XRD technique of Glavicic, *et al.* [6]: (a) measured  $\alpha_p + \alpha_s$  texture, (b) measured  $\alpha_p$  texture, and (b) calculated  $\alpha_s$  texture.

Figure 9. SEM BSE images of the microstructure developed in the starting (unrolled) Ti-6Al-4V program material during heat treatment at 955°C for 4 hours followed by (a) water quenching or (b) furnace cooling.

Figure 10. Alpha-phase (0001) pole figures determined by EBSD for the starting Ti-6Al4V plate heat treated 4 hours at 955°C followed by (a) water quenching or (b) furnace cooling. Scanned areas were 1.2 mm x 1.2 mm.

Figure 11. Alpha-phase (0001) pole figures determined by EBSD for the starting Ti-6Al4V plate heat treated 4 hours at 955°C followed by (a) water quenching or (b) furnace cooling. Scanned areas were 20 mm x 4.8 mm.

Figure 12. Rolling-direction IPF maps determined by EBSD for the starting Ti-6Al4V plate heat treated 4 hours at 955°C followed by (a) water quenching or (b) furnace cooling. Scanned areas were 1.2 mm x 1.2 mm. The rolling direction is horizontal.

Figure 13. Rolling-direction IPF maps determined by EBSD for the starting Ti-6Al4V plate heat treated 4 hours at 955°C followed by (a) water quenching or (b) furnace cooling.. Scanned areas were 20 mm x 4.8 mm. The rolling direction is horizontal.

Figure 14. Separation of  $\alpha_p$  and martensite using Image Quality determined by EBSD for the starting Ti-6Al4V plate heat treated 4 hours at 955°C followed by water quenching: (a) IQ map revealing  $\alpha_p$  as light gray areas and martensite as dark gray matrix (b) the corresponding microstructure partitioned based on IQ. In, (b),  $\alpha_p$  particles are painted blue. (c) Partitioned  $\alpha_p$  particles corresponding to the blue areas in (b).

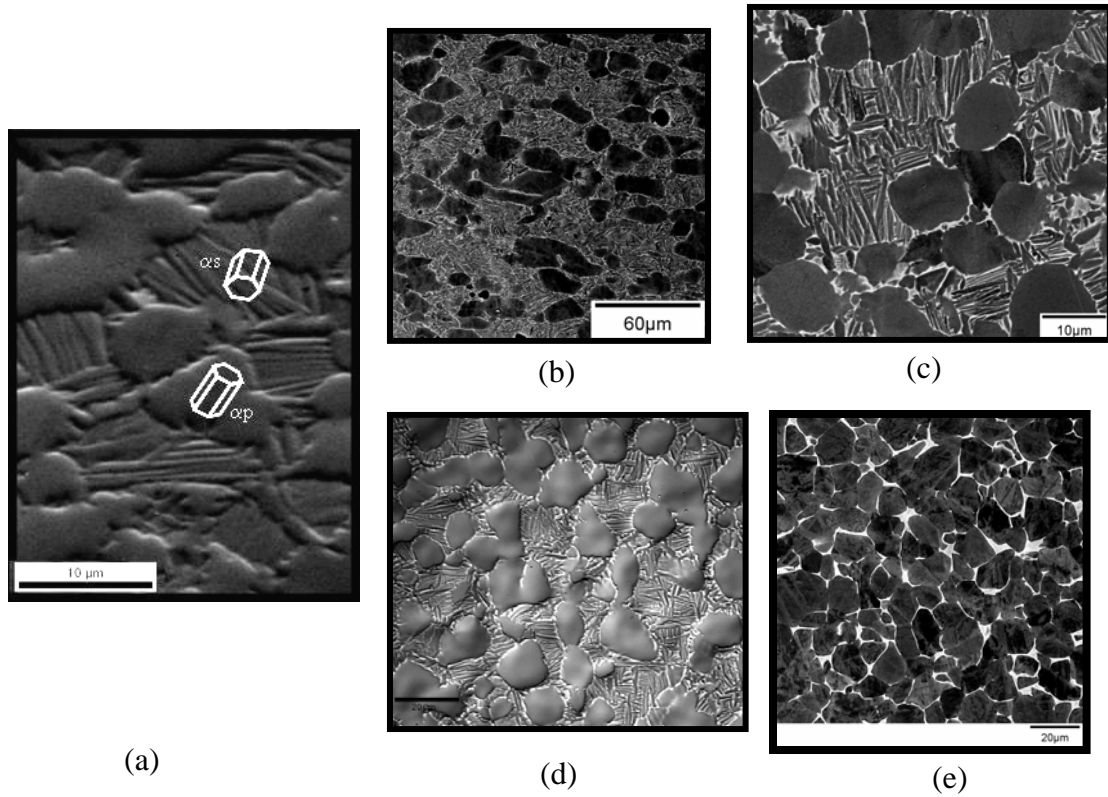


Figure 1. Ti-6Al-4V microstructures: (a) SEM secondary-electron image for material with a duplex microstructure of globular  $\alpha_p$  and colonies of  $\alpha_s$ , (b) low magnification backscattered-electron (BSE) image revealing  $\alpha_p$  particles as dark areas and  $\alpha_s$  colonies as light gray areas, (c) high magnification BSE image revealing the similarity in darkness of both  $\alpha_p$  particles and the  $\alpha_s$  in the lamellar colonies, (d) optical micrograph of electropolished-and-etched surface revealing  $\alpha_p$  particles and  $\alpha_s$  colonies and (e) BSE image of the sample after epitaxial growth of the  $\alpha_p$  particles via furnace cooling from the solution temperature

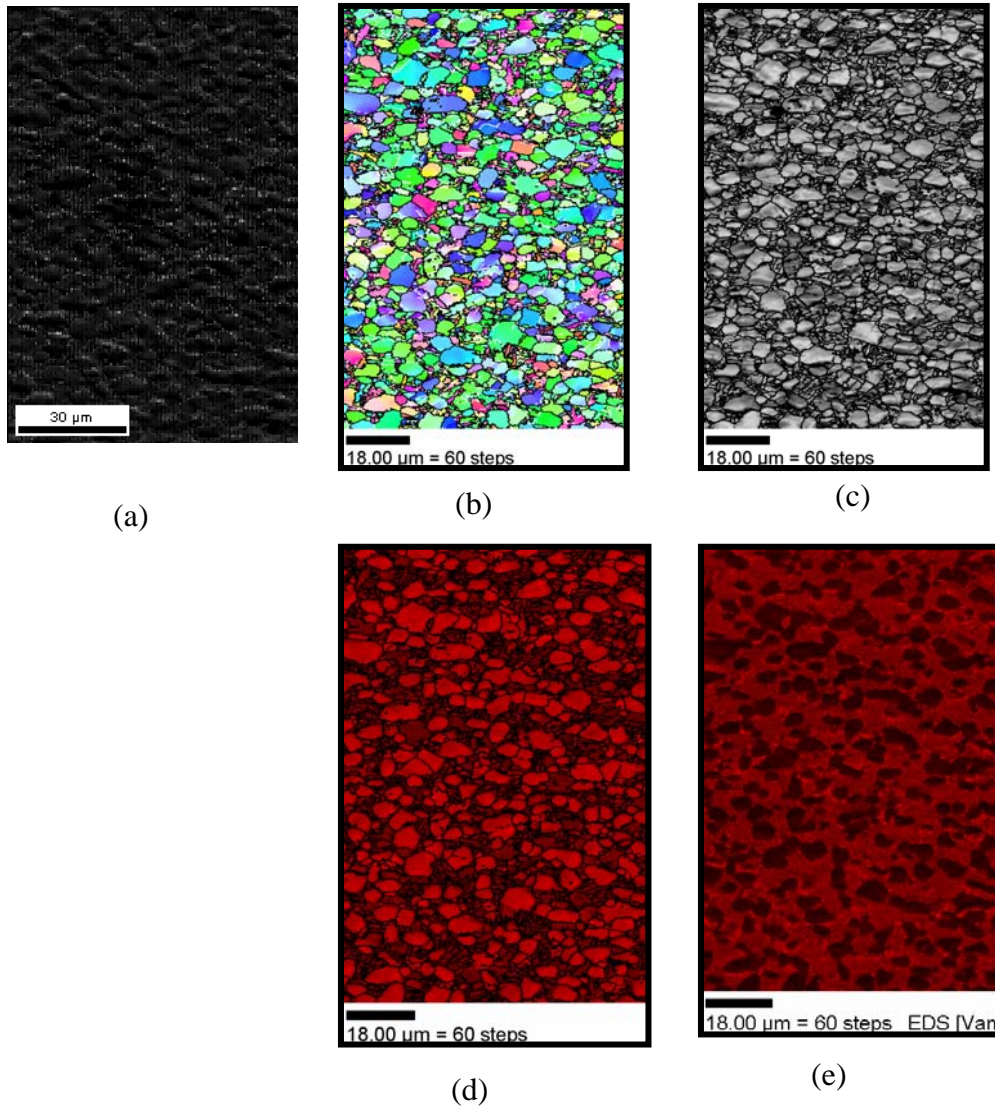


Figure 2. SEM results for an electropolished sample of hot-rolled Ti-6Al-4V: (a) secondary-electron image, (b) normal-direction inverse-pole-figure map showing indistinguishable  $\alpha_p$  and  $\alpha_s$  phases, (c) image-quality map of the same area with no clear difference between  $\alpha_s$  and  $\alpha_p$  phases, and EDS maps for (d) aluminum and (e) vanadium. In the EDS maps (d, e), dark or light shading is associated with lower or higher concentrations, respectively of the particular alloying elements.

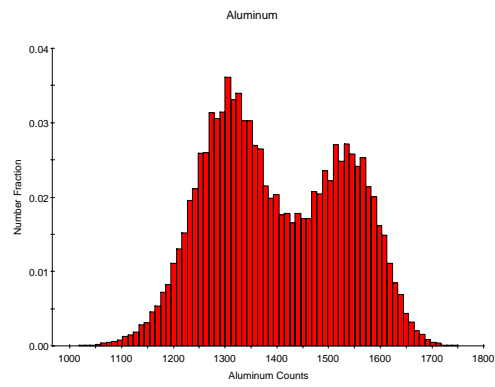
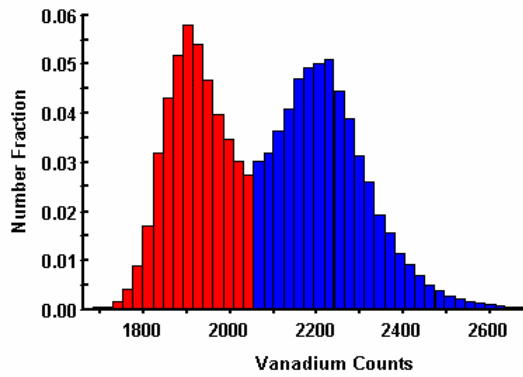
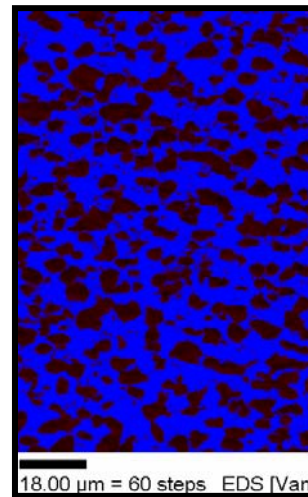


Figure 3. Aluminum histogram determined by EDS.



(a)



(b)

Figure 4. Separation of  $\alpha_p$  and  $\alpha_s$  using vanadium partitioning: (a) EDS histogram (b) the corresponding microstructure partitioned based on vanadium content. In, (b),  $\alpha_s$  colonies are painted blue.

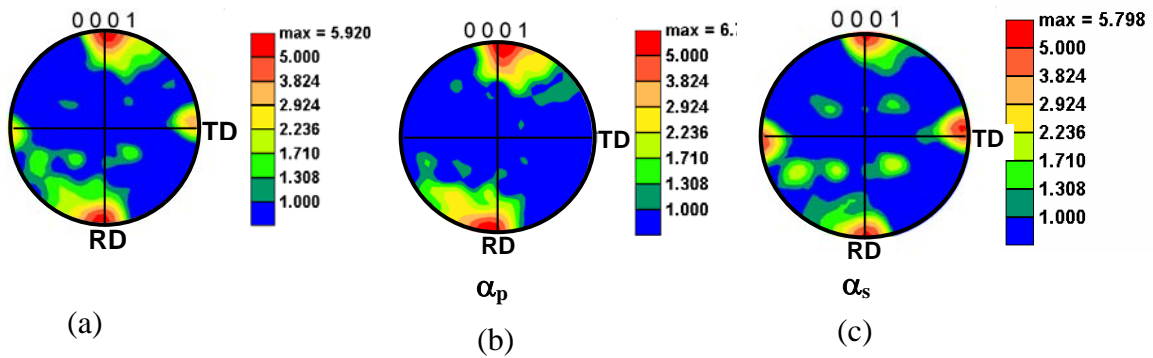


Figure 5. Alpha-phase (0001) pole figures for hot-rolled Ti-6Al-4V determined by the EBSD/EDS technique and vanadium partitioning: (a)  $\alpha_p + \alpha_s$  texture, (b)  $\alpha_p$  particles, and (c)  $\alpha_s$  colonies.

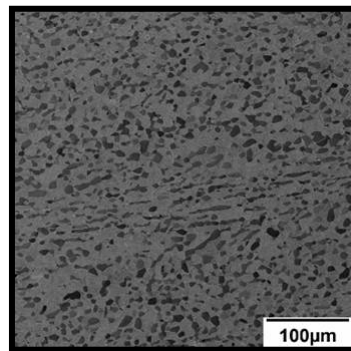


Figure 6. Backscattered-electron image of the microstructure developed in undeformed Ti-6Al-4V during solution treatment at the rolling temperature (955°C) followed by water quenching.

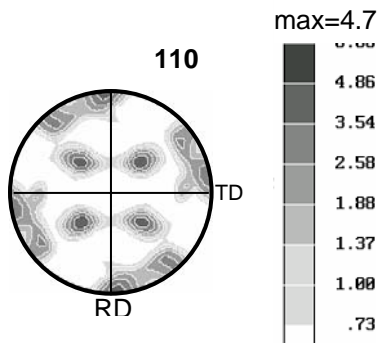


Figure 7. Beta-phase (110) pole figure for hot-rolled Ti-6Al-4V determined by XRD.

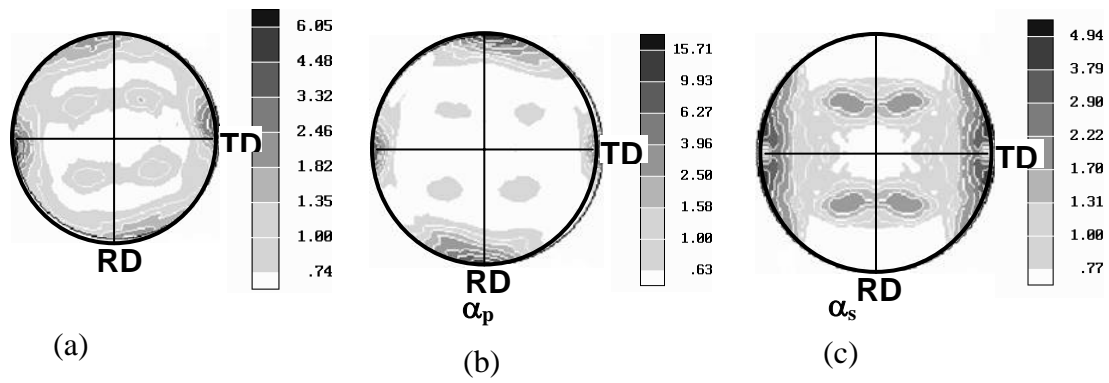


Figure 8. Alpha-phase (0001) pole figures for hot-rolled Ti-6Al-4V determined using the XRD technique of Glavicic, *et al.* [6]: (a) measured  $\alpha_p + \alpha_s$  texture, (b) measured  $\alpha_p$  texture, and (c) calculated  $\alpha_s$  texture.

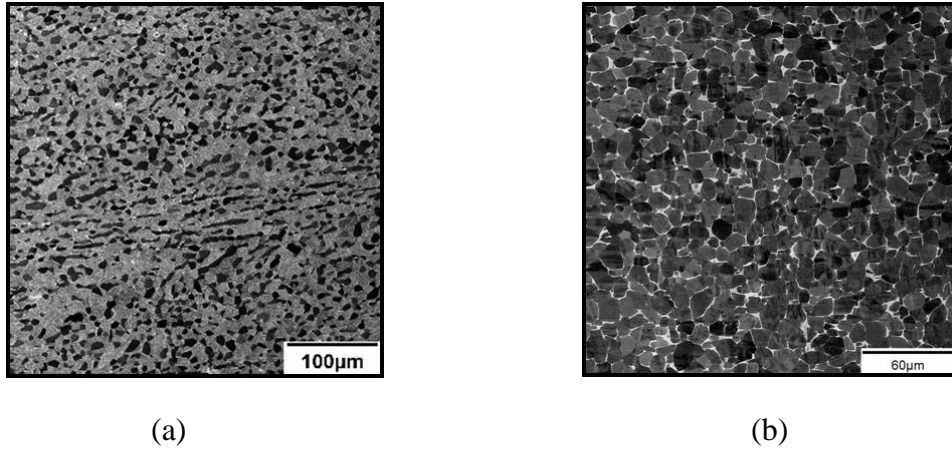


Figure 9. SEM BSE images of the microstructure developed in the starting (unrolled) Ti-6Al-4V program material during heat treatment at 955°C for 4 hours followed by (a) water quenching or (b) furnace cooling.

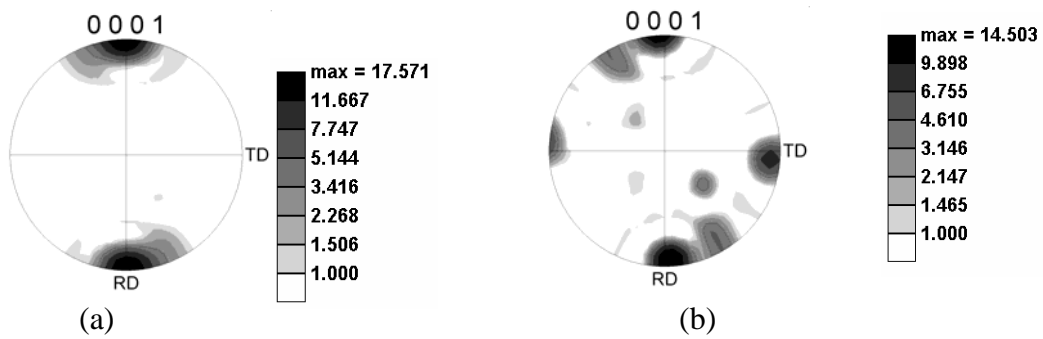


Figure 10. Alpha-phase (0001) pole figures determined by EBSD for the starting Ti-6Al-4V plate heat treated 4 hours at 955°C followed by (a) water quenching or (b) furnace cooling. Scanned areas were 1.2 mm x 1.2 mm.

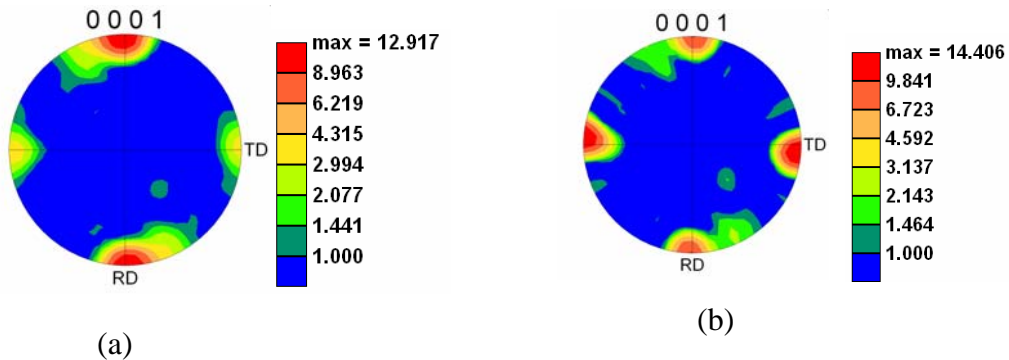


Figure 11. Alpha-phase (0001) pole figures determined by EBSD for the starting Ti-6Al-4V plate heat treated 4 hours at 955°C followed by (a) water quenching or (b) furnace cooling. Scanned areas were 20 mm x 4.8 mm.

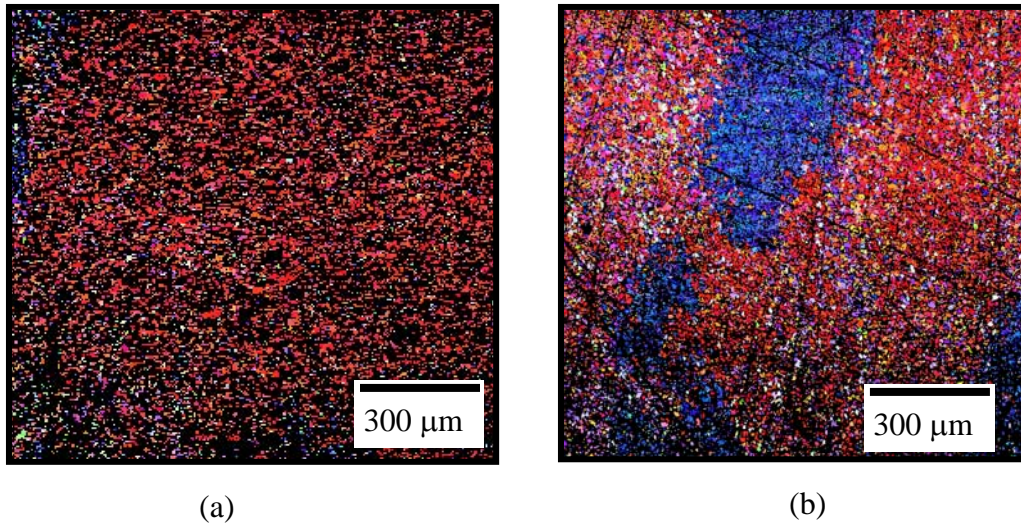


Figure 12. Rolling-direction IPF maps determined by EBSD for the starting Ti-6Al4V plate heat treated 4 hours at 955°C followed by (a) water quenching or (b) furnace cooling. Scanned areas were 1.2 mm x 1.2 mm. The rolling direction is horizontal.

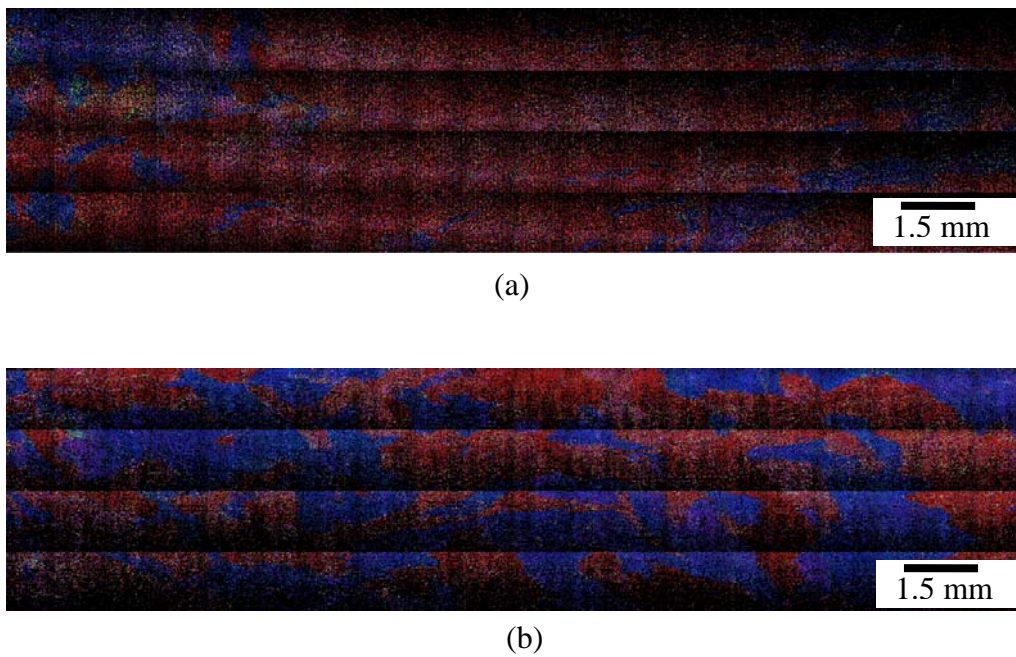
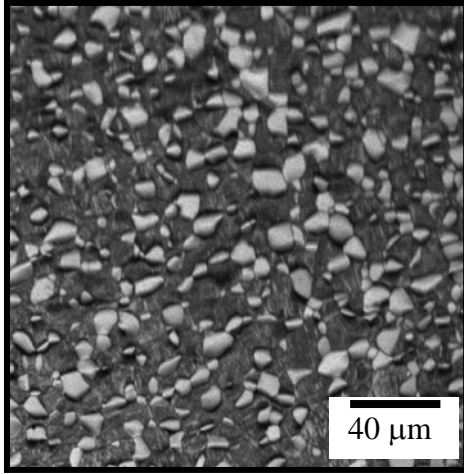
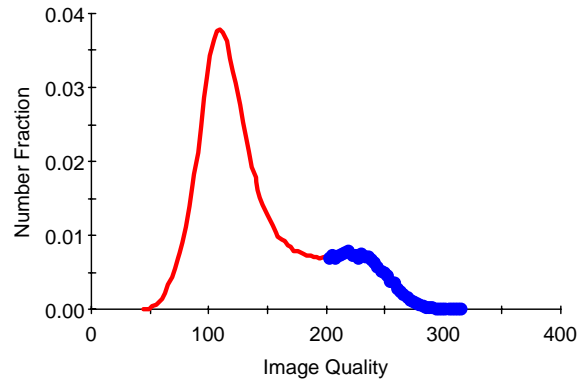


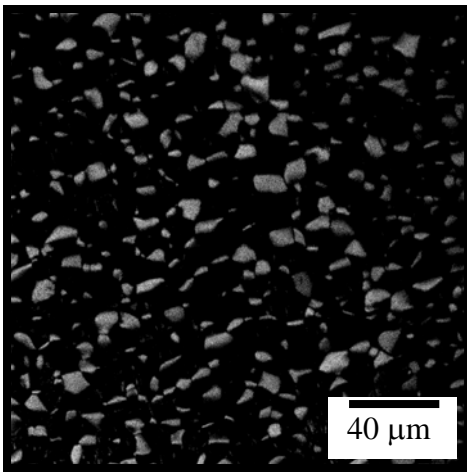
Figure 13. Rolling-direction IPF maps determined by EBSD for the starting Ti-6Al4V plate heat treated 4 hours at 955°C followed by (a) water quenching or (b) furnace cooling.. Scanned areas were 20 mm x 4.8 mm. The rolling direction is horizontal.



(a)



(b)



(c)

Figure 14. Separation of  $\alpha_p$  and martensite using Image Quality determined by EBSD for the starting Ti-6Al4V plate heat treated 4 hours at 955°C followed by water quenching: (a) IQ map revealing  $\alpha_p$  as light gray areas and martensite as dark gray matrix (b) the corresponding microstructure partitioned based on IQ. In, (b),  $\alpha_p$  particles are painted blue. (c) Partitioned  $\alpha_p$  particles corresponding to the blue areas in (b).